

Parallax of PSR J1744–1134 and the Local Interstellar Medium

M. Toscano^{1,2}, M. C. Britton², R. N. Manchester^{3,1}, M. Bailes², J. S. Sandhu⁴, S. R. Kulkarni⁴, S. B. Anderson⁴

¹Physics Department, University of Melbourne, Parkville, Vic 3052, Australia;
mtoscano@physics.unimelb.edu.au.

²Astrophysics and Supercomputing, Mail No. 31, Swinburne University of Technology,
PO Box 218, Hawthorn, Vic 3122, Australia; mbritton@pulsar.physics.swin.edu.au,
mbailes@swin.edu.au.

³Australia Telescope National Facility, CSIRO, PO Box 76, Epping, NSW 2121, Australia;
rmanches@atnf.csiro.au.

⁴Department of Astronomy, Caltech, Pasadena CA 91125; jss@astro.caltech.edu,
srk@astro.caltech.edu, sba@srl.caltech.edu.

Received _____; accepted _____

ABSTRACT

We present the annual trigonometric parallax of PSR J1744–1134 derived from an analysis of pulse times of arrival. The measured parallax, $\pi = 2.8 \pm 0.3$ mas ranks among the most precisely determined distances to any pulsar. The parallax distance of 357_{-35}^{+43} pc is over twice that derived from the dispersion measure using the Taylor & Cordes model for the Galactic electron distribution. The mean electron density in the path to the pulsar, $n_e = (8.8 \pm 0.9) \times 10^{-3}$ cm⁻³, is the lowest for any disk pulsar. We have compared the n_e for PSR J1744–1134 with those for another 11 nearby pulsars with independent distance estimates. We conclude that there is a striking asymmetry in the distribution of electrons in the local interstellar medium. The electron column densities for pulsars in the third Galactic quadrant are found to be systematically higher than for those in the first. The former correlate with the position of the well known local HI cavity in quadrant three. The excess electrons within the cavity may be in the form of HII clouds marking a region of interaction between the local hot bubble and a nearby superbubble.

Subject headings: pulsars: individual (PSR J1744–1134) — pulsars: general — ISM: general

1. Introduction

Among the fundamental building blocks of astronomy is the ability to measure reliable distances to objects of interest. These not only provide us with their location but also allow us to study properties that are functions of distance. Independent and consistent measurements of distances to local objects establish a distance scale upon which all greater distances are based. Precise, model-independent measurements of distances to pulsars are rare, yet they are an invaluable resource with which to study the interstellar medium (ISM). These pulsar distances provide information about the column density of free electrons along different lines-of-sight (LOSs).

Since their discovery, pulsars have had their distances estimated primarily by measuring the dispersion delay between pulses arriving at two widely spaced frequencies. As this delay is a function of the integral of electron density along the LOS to the pulsar, or dispersion measure (DM), a model for the Galactic free electron distribution yields the pulsar’s distance (e.g., Taylor & Cordes 1993). Pulsar distances have also been inferred from associations with objects with independently measured distances, e.g. globular clusters (Lyne 1995), supernova remnants (Kaspi 1996), and the Magellanic clouds (Feast 1991). When detection of neutral hydrogen (HI) absorption of the pulsar signal is possible, an estimate, or at least a limit on the distance may be obtained using a Galactic rotation model (e.g., Johnston et al. 1996).

The most direct estimate of distance to a pulsar is obtained from measurement of its annual trigonometric parallax, π . In practice, however, measuring π is difficult since it requires astrometric measurements with sub-milliarcsecond accuracy made over several years. To date parallaxes have been measured for only the 12 nearby pulsars listed in Table 1. Many of these parallaxes have

been obtained using long baseline interferometers (e.g., Gwinn 1984). In this Letter, we describe a measurement of the parallax of PSR J1744–1134 obtained by analysing pulse times of arrival (TOAs) spanning 4 years and combine this result with other similar measurements to study the electron distribution in the local ISM (LISM).

2. Observations, Analysis and Results

The timing measurements of PSR J1744–1134 were made as part of an ongoing millisecond pulsar (MSP) timing project using the 64-m Parkes radio telescope. We describe briefly the observational and analytic methodology used, while a detailed account is presented by Toscano et al. (1999).

Between 1995 January and 1999 January we made regular observations of PSR J1744–1134 at 0.66 and 1.4 GHz. At 0.66 GHz we used a dual linear polarization receiver. During the period of 1997 April until 1998 August we used the center beam of the Parkes Multibeam receiver system for dual linear polarization observations about 1.4 GHz. At other times observations at 1.4 GHz were made with a dual circular polarization H-OH receiver. The downconverted signal was fed into the Caltech correlator (Navarro 1994) where it was digitized and autocorrelated. The autocorrelation functions were folded at the topocentric pulse period, Fourier transformed, and compressed to 180 s sub-integrations, 8 frequency channels and 512 phase bins. A typical observation consisted of 8 contiguous sub-integrations. At 0.66 GHz, the signal was recorded over 32 MHz of bandwidth. Near 1.4 GHz we observed with two 128 MHz bands centered near 1.4 and 1.6 GHz respectively.

Profiles for each observation were formed by summing all frequency channels and sub-integrations. The highest signal-to-noise ratio (SNR) profiles were

added to form standard profiles for each observing frequency. After eliminating profiles with very low SNR and/or high levels of radio frequency interference we were left with 158 24-min integrated profiles. Pulse TOAs and TOA errors were determined by fitting these integrated profiles with the standard profile (Taylor 1990). Arrival-time data were fitted to a pulse timing model using the TEMPO program (<http://pulsar.princeton.edu/tempo/>). The JPL DE200 ephemeris (Standish 1982) was used to transform TOAs to the solar system barycenter.

The amplitude and functional form of the residuals from a least-squares fit to the TOAs of pulsar position, proper motion, pulse period and its first time derivative, and DM, with π set to zero is referred to as the ‘timing signal’ for parallax. The signal has a semi-annual period and amplitude $r^2 \cos^2 \theta / (2cd)$, where r is the Earth’s orbital radius, θ is the pulsar’s ecliptic latitude and d its distance (Ryba & Taylor 1991a). Thus, a timing precision of $\sim 1\mu\text{s}$ limits detection of π to pulsars $\lesssim 1$ kpc away.

The upper panel of Figure 1 shows the timing residuals of PSR J1744–1134 folded with a semi-annual period for a model fit excluding parallax. Also plotted is the timing signal corresponding to $\pi = 2.8$ mas — the best fit value for parallax. The residuals for a model fit including π are shown in the lower panel. The former fit resulted in a post-fit residual rms of $0.80\mu\text{s}$, while the latter produced an rms of $0.47\mu\text{s}$. Thus, the inclusion of parallax in the timing model yields a significant improvement to its accuracy. There are some indications of red noise in the TOAs in Figure 1. These systematics arise from inaccuracies in the calibration of pulse profiles, and introduce red noise in the TOAs on time-scales of hours (Britton 1999). Such short-term systematics average out over the semi-annual time-scale of parallax, and should not affect our measured value. Although the statistical error in π from the fit is 0.1 mas, the presence of

systematics in the residuals will tend to cause an underestimation of this error. To quantify the effects of systematics on our parallax error we divided our data into 4 sub-sets of 1 year. Fits to independent pairwise combinations of these sub-sets were consistent with $\pi = 2.8 \pm 0.3$ mas. To this precision timing noise does not contribute to the measured parallax. The 8 parameter values resulting from the best fit, along with derived parameters, are presented in Table 2.

3. Discussion

Our parallax measurement of PSR J1744–1134 places it at a distance of 357^{+43}_{-35} pc. This distance is over twice the value of 166 pc derived from the DM using the Taylor & Cordes (1993) model. The improved distance measurement implies a mean electron density in the path to the pulsar of $n_e = (8.8 \pm 0.9) \times 10^{-3}$ cm⁻³. This is the lowest n_e for any known pulsar with a low z -height. To determine whether this LOS is exceptional, we have compared n_e for PSR J1744–1134 with those of another 11 local ($d \lesssim 1$ kpc) pulsars with independent distance estimates. With the exception of PSRs J1024–0719, B1534+12, and B0833–45 (Vela) all such estimates were derived from parallax measurements (Table 1). A firm upper distance limit to PSR J1024–0719 of 226 pc results from assuming that its observed spin-down rate is entirely due to its transverse motion (Shklovskii effect; Shklovskii 1970). Note that this upper limit is $\sim 40\%$ lower than the DM derived distance. A distance to PSR B1534+12 of 1.1 ± 0.2 kpc (consistent with their parallax measurement) has been derived by Stairs et al. (1998) from a measured change in its orbital period derivative under the assumption that general relativity is correct. Recently, Cha, Sembach & Danks (1999) derived a distance to the Vela supernova remnant of 250 ± 30 pc — half the canonically accepted value (Milne 1968).

PSRs J1744–1134 and J1024–0719 are two of only three isolated MSPs detected at X-ray energies. Since these MSPs have similar spin parameters (Toscano et al. 1999), and presumably similar evolutionary histories, comparing their X-ray properties is useful in understanding the origin of their X-ray emission. With our revised distance estimates, the X-ray luminosity of PSR J1024–0719, $L_x < 1 \times 10^{29} d^2 \text{erg s}^{-1}$, is less than a third of the previously accepted value, and for PSR J1744–1134, $L_x = 4 \times 10^{29} d^2 \text{erg s}^{-1}$, is slightly higher than the previous value, and much larger than that of PSR J1024–0719 (cf. Becker & Trümper 1999).

When the distances to the sample of 12 local pulsars are projected onto the Galactic plane a striking asymmetry in the electron distribution becomes evident. Figure 2 depicts their projected positions and LOS electron densities. It is apparent that the LOS electron densities to pulsars in the third Galactic quadrant are systematically higher than those in the first. In general, densities in quadrants 1 and 3 are respectively lower and higher than values expected from the Taylor & Cordes model. Most of the 12 pulsars are close to and above the Galactic plane (z -heights < 200 pc, $b > 0$). PSRs J1713+0747 and B1534+12 are exceptional ($z = 473$ and 822 pc respectively) and therefore are expected to have low electron densities. PSRs J0437–4715, B0833–45 and PSR B1451–68 are the only pulsars at negative latitudes. The asymmetry may be more pronounced since the upper parallax limit of PSR B1929+10 sets an upper limit to its electron density ($n_e < 0.013 \text{ cm}^{-3}$), while the Shklovskii effect implies a firm lower bound to the n_e of PSR J1024–0719 ($n_e > 0.029 \text{ cm}^{-3}$).

The Taylor & Cordes model for the Galactic free electron distribution is generally reliable for distances $\gtrsim 1$ kpc. In the local region, the model electron density is uniform with $n_e = 0.02 \text{ cm}^{-3}$ in the Galactic plane; it takes no

account of the peculiar properties of the LISM. Independent distance limits to local pulsars are crucial to constraining the electron density in this region. With such constraints it may be possible to re-evaluate the DM derived distances to nearby pulsars. To further characterize the distribution of electrons in the LISM it is useful to relate their location to other interstellar features, such as bubbles, superbubbles, and clouds of neutral gas.

There is strong evidence for an elongated cavity in the neutral component of the LISM. This cavity surrounds the Sun and extends several hundred parsecs into quadrant 3 (Lucke 1978). The cavity appears as a region of low reddening extending 500 pc between $l = 210^\circ$ and 255° and 1.5 kpc toward $l = 240^\circ$. Running counter to this is very heavy obscuration beyond ~ 100 pc in the first quadrant. Similarly, HI column densities derived from ultraviolet observations show a marked paucity in HI along LOSs directed towards $l = 230^\circ$ (Frisch & York 1983; Paresce 1984). A similar morphology for this cavity is gleaned from NaI absorption measurements (Welsh et al. 1994). Figure 2 shows the position of the 12 pulsars with respect to the cavity in reddening material and HI. We note that pulsars with the highest electron column densities are located close to or within this cavity.

There are several features of interest within this cavity. One of these is the local hot bubble (LHB): a volume encompassing the Sun distinguished by low neutral gas densities and a 10^6 K, soft X-ray emitting gas (for reviews see Cox & Reynolds 1987; Breitschwerdt 1996). The size of the LHB may be estimated by assuming that its extent in any given direction is proportional to the intensity of soft X-rays from that part of the sky (Cox & Reynolds 1987; Snowden et al. 1990). A revision of this ‘displacement model’ based on *ROSAT* observations indicates that the LHB only partially fills the cavity (Snowden et al. 1998).

In some regions (e.g., quadrant 3) the boundary is not well defined because of enhancements in the X-ray emission from material thought to be not local. In this model the electron density inside the bubble is $n_e \sim 0.005 \text{ cm}^{-3}$. Recently Heiles (1998b) has provided evidence from HI, infrared, radio continuum and 0.25 keV X-ray observations for a superbubble in quadrant 3. This superbubble is centered at a distance of ~ 0.8 kpc in the direction of $l = 238^\circ$ — its nearest and farthest boundaries are about 0.2 and 1.3 kpc distant, respectively. Figure 2 shows that the local hot bubble and the superbubble fill much of the cavity, although the extent of the region between them is not well defined.

Electrons within the LHB contribute only a small amount to the DMs of local pulsars. Therefore, the large number of pulsars with lower than expected electron densities in quadrant 1 implies a dearth of ionized material in this quadrant at least out to ~ 1 kpc. This has implications for models of the Galactic magnetic field. The majority of rotation measurements (RMs) have been made to pulsars in quadrant 1. An analysis of RMs by Rand & Lyne (1994) has the uniform component of the local magnetic field directed towards $l \sim 90^\circ$ with a magnitude of $\sim 1.4 \mu\text{G}$. About 400 pc towards $l = 0^\circ$ the field direction reverses. Calibration of nearby pulsar distances is indispensable to mapping the large-scale RM changes that distinguish this effect.

The very high electron column densities toward PSRs B0823+26 (0.055 cm^{-3}), B0833–45 (0.270 cm^{-3}), B0950+08 (0.023 cm^{-3}) and J1024–0719 ($n_e > 0.029 \text{ cm}^{-3}$) in quadrant 3 indicate the presence of dense ionized gas immediately beyond the LHB. Alternatively, the LHB may have a much higher n_e , as in the model of Breitschwerdt & Schmutzler (1994). This could account for the nearby excess of electrons in quadrant 3 but would require a further reduction in electron density in quadrant 1. If the dense ionized material is

outside the LHB, the relative deficiency of electrons along the LOS to PSR J0437–4715 may be accounted for if the gas is clumped or has a non-uniform z -distribution. There is independent evidence for the existence of ionized clouds in this region. Gry, York & Vidal-Madjar (1985) and more recently Dupin & Gry (1998) have investigated the properties of highly ionized clouds along LOSs to β Canis Majoris ($l, b, d = 226^\circ, -14^\circ, 153$ pc). Gry et al. (1985) concluded that HII with $n_e = 0.07\text{-}0.14$ cm $^{-3}$ fills 40-90 pc of the β CMA LOS. Dupin & Gry (1998) find that two clouds dominate this LOS. They have also postulated that these clouds are in the process of cooling and recombining after having been shocked and ionized by some violent event. It is possible that this highly ionized region is associated with an interaction between the LHB and the superbubble.

4. Conclusion

We have measured a parallax of 2.8 ± 0.3 mas for PSR J1744–1134 based on analysis of pulse arrival time data. The corresponding distance of 357_{-35}^{+43} pc is more than twice that derived from the DM using the Taylor & Cordes (1993) electron density model. The derived electron density, $n_e = (8.8 \pm 0.9) \times 10^{-3}$ cm $^{-3}$, is the lowest of any pulsar close to the Galactic equator. We compared the LOS electron density to PSR J1744–1134 with those to another 11 nearby pulsars with independent distance estimates. We conclude that there is a striking asymmetry in the distribution of electrons in the LISM, with electron densities for pulsars in the third Galactic quadrant systematically higher than those in the first. We speculate that these ionized regions are associated with interactions at the boundary between the LHB and the more distant superbubble.

The authors thank the referee, whose insightful comments contributed to the

clarity of this paper.

REFERENCES

- Backer, D. C. & Sramek, R. A. 1982, *ApJ*, 260, 512.
- Bailes, M., Manchester, R. N., Kesteven, M. J., Norris, R. P., & Reynolds, J. E. 1990, *Nature*, 343, 240.
- Becker, W. & Trümper, J. 1999, *A&A*, 341, 803.
- Breitschwerdt, D. & Schmutzler, T. 1994, *Nature*, 371, 774.
- Breitschwerdt, D. 1996, *Space Sci. Rev.*, 78, 173.
- Britton, M. C. 1999, *ApJ*, submitted.
- Cambell, R. M., Bartel, N., Shapiro, I. I., Ratner, M. I., Cappollo, R. J., Whitney, A. R., & Putnam, N. 1996, *ApJ*, 136, 95.
- Camilo, F., Foster, R. S., & Wolszczan, A. 1994, *ApJ*, 437, L39.
- Cha, A. N., Sembach, K. R., & Danks, A. C. 1999, *ApJ*, 515, L25.
- Cox, D. P. & Reynolds, R. J. 1987, *ARA&A*, 25, 303.
- Dupin, O. & Gry, C. 1998, *A&A*, 335, 661.
- Feast, M. W. 1991, in *IAU Symposium No. 148: The Magellanic Clouds*, ed. R. Haynes & D. Milne, (Dordrecht: Reidel), p. 1.
- Fomalont, E. B., Goss, W. M., Beasley, A. J., & Chatterjee, S. 1999, *ApJ*, submitted.
- Frisch, P. C. & York, D. G. 1983, *ApJ*, 271, L59.
- Gry, C., York, D. G., & Vidal-Madjar, A. 1985, *ApJ*, 296, 593.
- Gwinn, C. R. 1984. PhD thesis, Princeton University.
- Gwinn, C. R., Taylor, J. H., Weisberg, J. M., & Rawley, L. A. 1986, *AJ*, 91, 338.

- Heiles, C. 1998a, in IAU Colloquium No. 166: The Local Bubble & Beyond: Lyman-Spitzer Colloquium, ed. D. Breitschwerdt, M. J. Freyberg, & J. Truemper, (Berlin: Springer-Verlag), p. 229.
- Heiles, C. 1998, *ApJ*, 498, 689.
- Johnston, S., Koribalski, B. S., Weisberg, J., & Wilson, W. 1996, *MNRAS*, 279, 661.
- Kaspi, V. M. 1996, in Pulsars: Problems and Progress, IAU Colloquium 160, ed. M. Bailes, S. Johnston, & M. Walker, Astronomical Society of the Pacific, 375.
- Kaspi, V. M., Taylor, J. H., & Ryba, M. 1994, *ApJ*, 428, 713.
- Lucke, P. B. 1978, *A&A*, 64, 367.
- Lyne, A. G. 1995, in Millisecond Pulsars - A Decade of Surprise, ed. A. S. Fruchter, M. Tavani, & D. C. Backer, volume 72, Astronomical Society of the Pacific, p. 35.
- Milne, D. K 1968, *Australian J. Phys.*, 21, 201.
- Navarro, J. 1994. PhD thesis, California Institute of Technology.
- Paresce, F. 1984, *AJ*, 89, 1022.
- Rand, R. J. & Kulkarni, S. R. 1989, *ApJ*, 343, 760.
- Rand, R. J. & Lyne, A. G. 1994, *MNRAS*, 268, 497.
- Ryba, M. F. & Taylor, J. H. 1991a, *ApJ*, 371, 739.
- Salter, M. J., Lyne, A. G., & Anderson, B. 1979, *Nature*, 280, 477.
- Sandhu J. S., Bailes M., Manchester R. N., Navarro J., Kulkarni S. R., Anderson S. B., 1997, *ApJ*, 478, L95
- Shklovskii, I. S. 1970, *Soviet Astron.*, 13, 562.

- Snowden, S. L., Cox, D. P., McCammon, D., & Sanders, W. T. 1990, *ApJ*, 354, 211.
- Snowden, S. L., Egger, R., Finkbeiner, D. P., Freyberg, M. J., & Plucinsky, P. P. 1998, *ApJ*, 493, 715.
- Stairs, I. H., Arzoumanian, Z., Camilo, F., Lyne, A. G., Nice, D. J., Taylor, J. H., & Wolszczan, A. 1998, *ApJ*, 505, 352.
- Stairs, I. H., Thorsett, S. E., & Camilo, F. 1998, *ApJS*, in press.
- Standish, E. M. 1982, *A&A*, 114, 297.
- Taylor, J. H. 1990, in *Workshop on Impact of Pulsar Timing on Relativity and Cosmology*, ed. D. C. Backer, University of California Berkeley, p. m7.
- Taylor, J. H. & Cordes, J. M. 1993, *ApJ*, 411, 674.
- Toscano, M., Sandhu, J. S., Bailes, M., Manchester, R. N., Britton, M. C., Kulkarni, S. R., Anderson, S. B., & Stappers, B. W. 1999, *MNRAS*, in press.
- Welsh, B. Y., Craig, N., Vedder, P. W., & Vallergera, J. V. 1994, *ApJ*, 437, 638.
- Xilouris, K. M., Kramer, M., Jessner, A., von Hoensbroech, A., Lorimer, D. R., Wielebinski, R., Wolszczan, A., & Camilo, F. 1998, *ApJ*, 501, 286.

Figure Captions

Figure 1. Timing residuals for PSR J1744–1134. The upper panel shows residuals for frequencies centered at 0.66 (triangles) and about 1.4 GHz (circles), after fitting a timing model excluding parallax. The residuals have been folded at a period of 0.5 years and the sinusoid corresponds to the form and magnitude of a parallax of 2.8 mas. The lower panel displays the residuals after fitting for this parallax.

Figure 2. Features in the local ISM projected on to the Galactic plane. The Sun is located at the origin with concentric annuli at 200 pc intervals. The position of 12 pulsars are marked by circles, with radii proportional to the mean electron density in the path to the pulsar. The exceptionally large n_e for Vela is marked with a circled ‘V’ centered on its position. Letters refer to the pulsars listed below the figure, and electron densities (in units of cm^{-3}) are quoted alongside each pulsar. The positive and negative signs superposed on C and E points indicate lower and upper bounds, respectively. Note the asymmetric distribution of electron density. Contours plotted as solid lines indicate color excess (Lucke 1978; Figure 5). The innermost contour level is $E(B - V) = 0.1$ and the levels increase outward in steps of 0.1 mag. Depressed contours are indicated by tick marks. The contour plotted as a dashed line indicates the neutral hydrogen column density with a level of $N(\text{HI}) = 5 \times 10^{19} \text{ cm}^{-2}$ (Frisch & York 1983; Figure 1c). The cross-section of the LHB through the Galactic plane is shown as a shaded patch at the Sun’s location (Snowden et al. 1998; Figure 11). The superbubble identified by Heiles (1998b) is plotted as a shaded ellipse. We note that the high electron densities correlate with the position of the HI cavity and with the region between the LHB and the superbubble.

Table 1. Parallax and Distance to 12 Pulsars

Pulsar	π mas	l	b	Distance pc	Reference
J0437–4715	5.6 ± 0.8	253.4	–41.96	179^{+29}_{-23}	8
B0823+26	2.8 ± 0.6	197.0	31.7	357^{+97}_{-63}	6
B0919+06	0.31 ± 0.14	225.4	36.4	3200^{+2700}_{-1000}	5
B0950+08	7.9 ± 0.8	228.9	43.7	127^{+14}_{-12}	6
B1451–68	2.2 ± 0.3	313.9	–8.5	455^{+70}_{-56}	2
B1534+12	<1.7	19.9	48.3	>588	9
J1713+0747	0.9 ± 0.3	28.8	25.2	1111^{+556}_{-278}	4
J1744–1134	2.8 ± 0.3	14.8	9.2	357^{+43}_{-35}	...
B1855+09	1.1 ± 0.3	42.3	3.1	909^{+341}_{-195}	7
B1929+10	<4 ^a	47.4	–3.9	>250	1
B1937+21	<0.28	57.5	–0.3	>3571	7
B2021+51	0.95 ± 0.37	87.9	8.4	1050^{+250}_{-150}	3

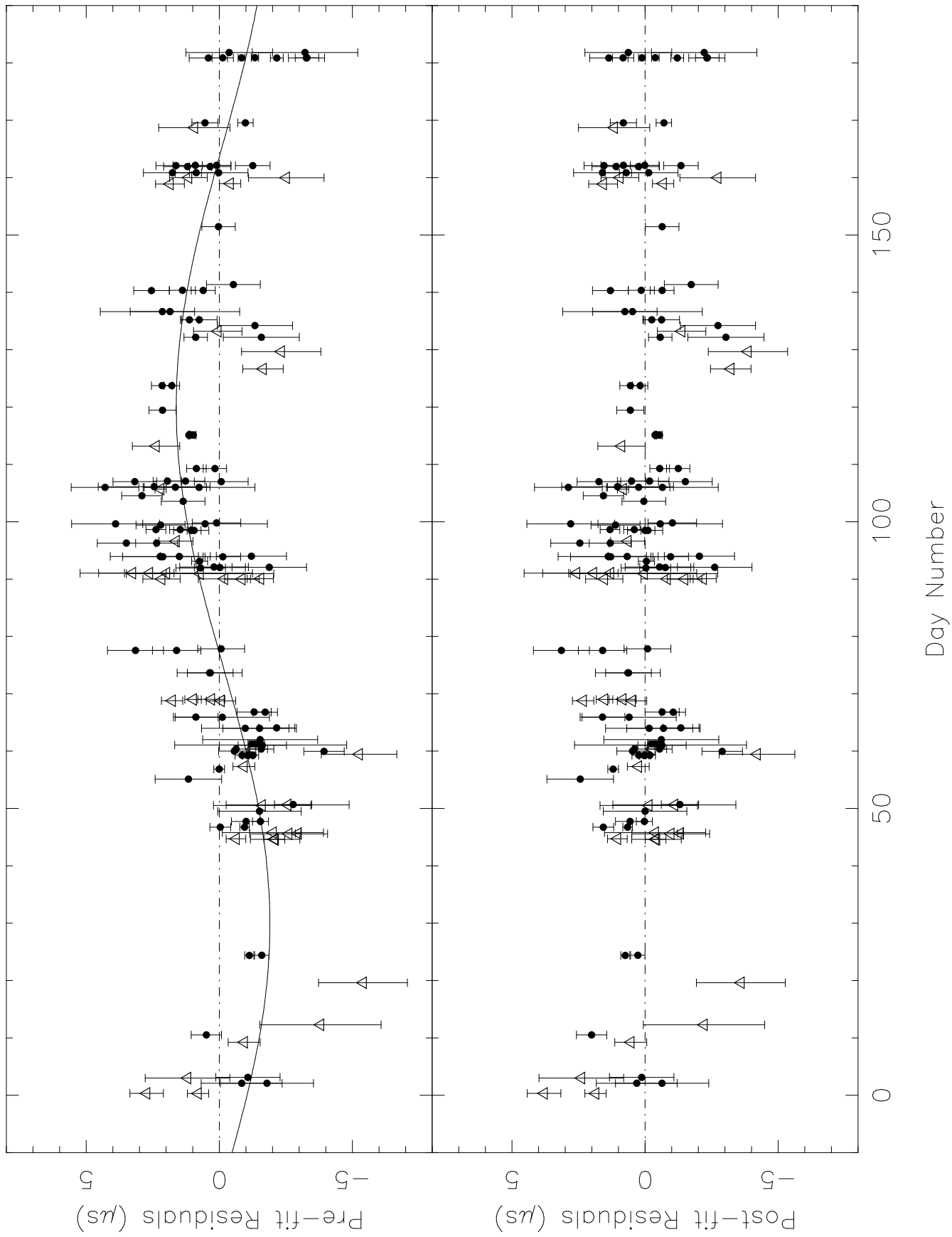
^aA measurement of 21.5 ± 0.3 mas by Salter, Lyne, & Anderson (1979) was not included in our analysis.

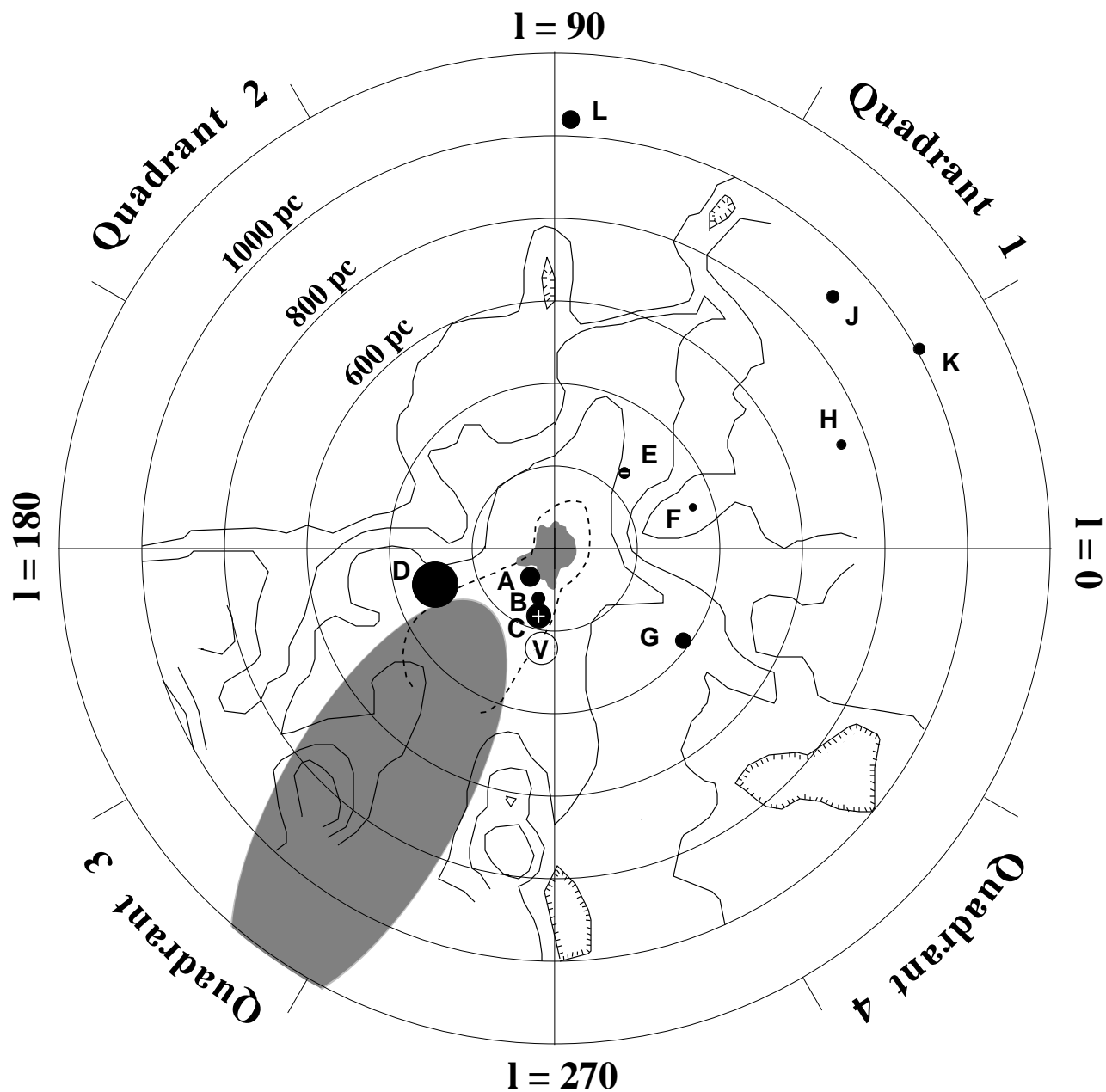
References. — (1) Backer & Sramek 1982; (2) Bailes et al. 1990; (3) Cambell et al. 1996; (4) Camilo, Foster, & Wolszczan 1994; (5) Fomalont et al. 1999; (6) Gwinn et al. 1986; (7) Kaspi, Taylor, & Ryba 1994; (8) Sandhu et al. 1997; (9) Stairs et al. 1998

Table 2. Observed and Derived Parameters for PSR J1744–1134

Parameter	Value ^a
R. A. (J2000)	17 ^h 44 ^m 29 ^s .390963(5)
Decl. (J2000)	–11° 34′ 54″.5746(5)
Proper motion in R.A. (mas y ^{–1})	18.72(6)
Proper motion in Decl. (mas y ^{–1})	–9.5(4)
Annual parallax (mas)	2.8(3)
Period, P (ms)	4.07454587512695(3)
Period derivative, \dot{P} (10 ^{–20})	0.89405(9)
Epoch of period and position (MJD)	50434.0
Dispersion Measure (cm ^{–3} pc)	3.1388(3)
Timing data span (MJD)	49730 – 51209
RMS timing residual (μ s)	0.47
Number of timing points	158
Galactic latitude & longitude (l, b)	14.79, 9.18
Parallax distance (pc)	357 ⁺⁴³ _{–35}
DM derived distance (pc)	166
\dot{P} upper distance limit (pc)	1910
Composite proper motion (mas y ^{–1})	21.0(2)
Celestial position angle of proper motion (deg)	116.8(9)
Transverse Velocity (km s ^{–1})	36(4)

^aFigures in parentheses represent 1σ uncertainties in the last digit quoted





A	B0950+08	0.023	E	B1929+10	<0.013	J	B1855+09	0.015
B	J0437-4715	0.015	F	J1744-1134	0.009	K	J1713+0747	0.014
C	J1024-0719	>0.029	G	B1451-68	0.019	L	B2021+51	0.021
D	B0823+26	0.055	H	B1534+12	0.011	Ⓟ	B0833-45	0.270